ACS APPLIED MATERIALS & INTERFACES

Research Article

www.acsami.org

Rational Design of Multifunctional Gold Nanoparticles via Host–Guest Interaction for Cancer-Targeted Therapy

Wei-Hai Chen, Qi Lei, Guo-Feng Luo, Hui-Zhen Jia, Sheng Hong, Yu-Xin Liu, Yin-Jia Cheng, and Xian-Zheng Zhang*

Key Laboratory of Biomedical Polymers of Ministry of Education & Department of Chemistry, Wuhan University, Wuhan 430072, China

Supporting Information

ABSTRACT: A versatile gold nanoparticle-based multifunctional nanocomposite AuNP@CD-AD-DOX/RGD was constructed flexibly via host–guest interaction for targeted cancer chemotherapy. The pH-sensitive anticancer prodrug AD-Hyd-DOX and the cancer-targeted peptide AD-PEG$_8$-GRGDS were modified on the surface of AuNP@CD simultaneously, which endowed the resultant nanocomposite with the capability to selectively eliminate cancer cells. In vitro studies indicated that the AuNP@CD-AD-DOX/RGD nanocomposite was preferentially uptaken by cancer cells via receptor-mediated endocytosis. Subsequently, anticancer drug DOX was released rapidly upon the intracellular trigger of the acid microenvironment of endo/lysosomes, inducing apoptosis in cancer cells. As the ideal drug nanocarrier, the multifunctional gold nanoparticles with the active targeting and controllable intracellular release ability hold the great potential in cancer therapy.

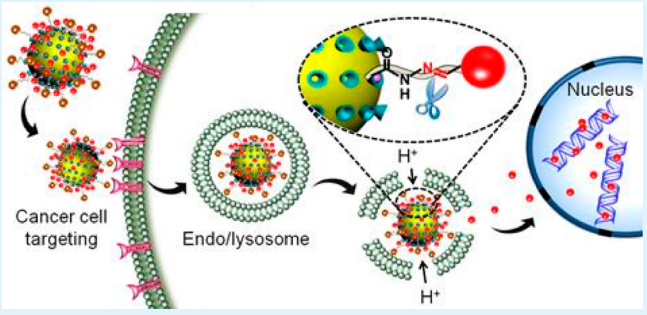

KEYWORDS: *Multifunctional, gold nanoparticles, host–guest interaction, targeted therapy, triggered release*

1. INTRODUCTION

There has been increased interesting in design of nanotechnology-based drug delivery system for cancer therapy since functional nanoparticles (magnetic nanoparticles, silica nanoparticles, and gold nanoparticles) are urgently expected to overcome the nonselectivity of chemotherapeutic agents, avoid the undesirable side effects, and improve the therapeutic outcomes of cancer therapy.[1−3] Inspired by the easy fabrication and convenient surface functionalization, gold nanoparticles (AuNPs) with excellent biocompatibility have been extensively used as nanocarriers for drug and gene delivery and diagnostic agents for imaging and sensing.[4−6] Especially, despite that the ultrasmall gold nanoparticles (2−4 nm) are expected to be rapidly excreted via kidney, they have been demonstrated to possess unique advantages, such as increasing cancer cells uptake and improving tumor permeability, which are beneficial to potentiate the therapeutic effect of anticancer drugs.[7−10] Although the functionalized AuNPs have achieved encouraging therapeutic effects in vitro and in vivo, the fabrication of ingenious drug carriers based on AuNPs with specific targeting and controllable release capability is still a critical challenge.

To realize the specific targeting delivery, the traditional strategy is to employ active targeting ligands to functionalize the carriers for specifically binding receptors overexpressed on the membrane of cancer cells.[11−14] To controllably release the drug, the sophisticated strategy is to trigger the release of drug at pathological sites in response to the particular stimuli, such as pH, light, temperature, enzymes, and so on.[15−18] Among these stimuli, pH-responsive drug delivery systems exhibit great promising to optimize the therapeutic efficacy of anticancer drugs and prevent the inevitable off-target release of drug since the pH values in cancerous tissues (pH 6.5) and intracellular endo/lysosomes (pH 4.0−6.0) are intrinsically lower than that in blood and normal tissues (pH 7.4).[19−24] However, it is difficult and complicated to introduce multiple functional moieties into a single gold nanoparticle without losing individual specialties of each component.

Recently, it is well-known that supramolecular chemistry, based on the modularized and specific noncovalent interaction, can connect host and guest molecules together and form stable inclusion complexes efficiently.[25−28] More importantly, the convenient and flexible host–guest interaction has been recognized as an important approach to improve and expand the design of functional delivery systems, which provides a great opportunity to construct multifunctional nanoparticles.[29,30] Based on the host–guest interaction, the different functional moieties can assemble into one carrier conveniently. For instance, cyclodextrin-modified gold nanoparticles have been applied to construct versatile platform via host–guest interaction for targeted drug delivery conveniently.[31,32]

Herein, a multifunctional nanocomposite based on β-cyclodextrin-modified gold nanoparticle (AuNP@CD) was

Received: May 10, 2015
Accepted: July 20, 2015
Published: July 20, 2015

DOI: 10.1021/acsami.5b04031
ACS Appl. Mater. Interfaces 2015, 7, 17171−17180

delicately designed and fabricated for cancer-targeted therapy with intracellular pH-triggered drug delivery. As shown in Scheme 1, the peptidic derivative adamantane−PEG_8−glycine−

Scheme 1. Schematic Illustration of the Formation of Multifunctional Nanocomposite and Cancer-Targeted Intracellular Drug Delivery[a]

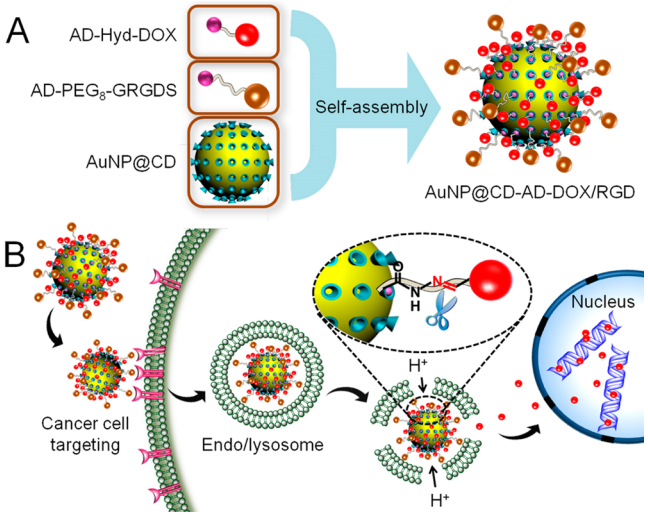

[a](A) The AD-PEG_8-GRGDS and AD-Hyd-DOX were flexibly self-assembled on the surface of AuNP@CD via host−guest interaction and facilely constituted the cancer-targeted nanocomposite AuNP@CD-AD-DOX/RGD. (B) The multifunctional nanocomposite was selectively uptaken by cancer cell via the active targeting strategy and the acid microenvirenment of endo/lysosomes triggered the rapid release of anticancer drug for cancer therapy.

arginine−glycine−aspartic−serine (AD-PEG_8-GRGDS) and the adamantane conjugated anticancer drug doxorubicin with hydrazone bond linkage (AD-Hyd-DOX) were decorated on the surface of AuNP@CD via host−guest interaction simultaneously, forming multifunctional nanocomposite AuNP@CD-AD-DOX/RGD. Since RGD peptide sequence can target cancer cells with overexpressed $\alpha_v\beta_3$ integrin,[33,34] AuNP@CD-AD-DOX/RGD would preferentially enter into cancer cells and significantly enhance cellular uptake for cancer-targeted drug delivery via receptor-mediated endocytosis. Once internalized in cancer cell and localized in endo/lysosomes, the anticancer drug would be released rapidly from AuNP@CD-AD-DOX/RGD due to the cleavage of acid−labile hydrazone linkage between adamantane and doxorubicin. Then the cancer cells were selectively eliminated by the activated drug. The designed multifunctional nanocomposite AuNP@CD-AD-DOX/RGD would effectively enhance anticancer efficacy due to the combination of promoted cellular uptake and subsequent rapid intracellular drug release.

2. EXPERIMENTAL SECTION

2.1. Materials. *N*-Fluorenyl-9-methoxycarbonyl (Fmoc) protected L-amino acids (Fmoc-Gly-OH, Fmoc-Arg(Pbf)−OH, Fmoc-Asp(OtBu)−OH, and Fmoc-Ser(tBu)−OH, 2-chlorotrityl chloride resin (100−200 mesh, loading: 0.4 mmol/g, 1% DVB), benzotriazol-1-yl-oxytripyrrolidinophosphonium hexafluorophosphate (PyBOP), *o*-benzotriazole-*N*,*N*,*N*′,*N*′-tetramethyluroniumhexafluorophosphate (HBTU), 1-hydroxybenzotriazole (HOBt), triisopropylsilane (TIS), and piperidine were purchased from GL Biochem. Ltd. (Shanghai, China) and used as received. Diisopropylethylamine (DIEA) was acquired from GL Biochem. Ltd. (Shanghai, China) and used after distillation. Fmoc-PEG_8-COOH was provided by Zhoubei Technology Co. Ltd. (Hangzhou, China). Trifluoroacetic acid (TFA), anhydrous ether, ninhydrin, sodium borohydride ($NaBH_4$), and gold(III) chloride trihydrate were obtained from Shanghai Chemical Co. (Shanghai, China) and used directly. Mono-6-ethylenediamine-β-CD was synthesized according to our previous literature procedures.[35] Adamantane chloride was purchased from Aladdin Reagent Co. Ltd. (Shanghai, China). *N*,*N*-Dimethylformamide (DMF), dimethyl sulfoxide (DMSO), methanol, and dichloromethane (DCM) were provided by Shanghai Chemical Co. (Shanghai, China) and distilled prior to use.

Doxorubicin hydrochloride was purchased from Zhejiang Hisun Pharmaceutical Co. (Zhejiang, China). 3-[4,5-Dimethylthiazol-2-yl]-2,5-diphenyltetra-zolium bromide (MTT), fetal bovine serum (FBS), penicillin streptomycin, trypsin, molecular probe (Hoechst 33342), and Dulbecco's phosphate buffered saline (PBS) were purchased from Invitrogen (USA). All other reagents and solvents were of analytical grade and used directly.

2.2. Synthesis of the Peptide Derivative Adamantane−PEG_8−Glycine−Arginine−Glycine−Aspartic−Serine (AD-PEG_8-GRGDS). The peptide derivative adamantane−PEG_8−glycine−arginine−glycine−aspartic−serine was synthesized by standard Fmoc solid phase peptide synthesis.[36] Briefly, peptide chains were grown on 2-chlorotriyl chloride resin. The coupling of the first residue used 4 equiv (relative to the substitution degree of resin) of Fmoc-protected amino acid and 6 equiv of DIEA in a DMF solution for 2 h. Other amino acid couplings were implemented with 4 equiv of Fmoc-protecting amino acid, 4 equiv of HBTU, and 6 equiv of DIEA in a DMF solution for 4 h. During the synthesis, Fmoc protected groups were deprotected by 20% piperidine/DMF (v/v) for twice and every time for 15 min. At the end of the synthesis, adamantane chloride was conjugated to the peptide segments. After the completion of the synthesis, the resin was finally washed with DMF (four times) and DCM (four times) and dried under vacuum for 24 h. Cleavage of the expected peptide and the removal of side chain protected groups from the dried resin were performed by suspending the resin in a cleavage cocktail containing TFA (95%), TIS (2.5%), and H_2O (2.5%) for 2 h. The filtration was concentrated to a viscous solution by rotary evaporation. After precipitating in cold ether, the crude product was collected and vacuum-dried. Then the crude product was dissolved in distilled water and freeze-dried. The molecular weight of AD-PEG_8-GRGDS was determined by ESI-MS (Finnigan LCQadvantage). The calculated molecular mass of AD-PEG_8-GRGDS was 1075.6 and the ESI-MS result found to be 1075.5 (Figure S1). The structure of AD-PEG_8-GRGDS was confirmed by ^{1}H NMR (Figure S7) and ^{13}C NMR (Figure S8). ^{1}H NMR (DMSO-d_6, 300 MHz, Figure S7) δ 0.81−0.87 ppm (s, 2H), 1.04−1.79 ppm (m, 16H), 1.88−2.03 ppm (m, 4H), 3.03−3.21 ppm (m, 4H), 3.58−3.88 ppm (m, 32H), 4.10−4.33 ppm (m, 5H), 4.52−4.62 ppm (s, 2H), 7.14−7.46 ppm (m, 2H), 7.77−8.37 ppm (m, 3H). ^{13}C NMR (DMSO-d_6, 300 MHz, Figure S8) δ 25.2 ppm, 28.2 ppm, 29.5 ppm, 35.9 ppm, 36.6 ppm, 42.3 ppm, 50.2 ppm, 52.6 ppm, 55.6 ppm, 61.6 ppm, 67.2 ppm, 70.1 ppm, 157.1 ppm, 169.8 ppm, 170.9 ppm, 172.4 ppm, 177.4 ppm. In the ^{1}H NMR spectrum of AD-PEG_8-GRGDS, the characteristic signals at δ 1.04−1.79 ppm belonging to AD and the abundant proton signal of PEG (δ 3.58−3.88 ppm) were clearly detectable. Simultaneously, the ^{13}C signals (δ < 40 ppm) attributed to AD and the ^{13}C signals of PEG skeleton (δ 70.1 ppm) as well as the ^{13}C signals of the amino acid skeleton (δ 169.8 ppm, 170.9, 172.4, and 177.4 ppm) were detected in the ^{13}C NMR spectrum of AD-PEG_8-GRGDS. These results indicated that AD-PEG_8-GRGDS have been synthesized successfully.

2.3. Synthesis of Adamantane Hydrazone Bond Linked Anticancer Drug Doxorubicin (AD-Hyd-DOX). First, AD-NH-NH_2 was synthesized according to the established procedure with some minor modifications.[37] In brief, hydrazine (0.5 mL, 99%) was dissolved in 15 mL of dry tetrahydrofuran. Subsequently, 10 mL of dry tetrahydrofuran containing 1.0 g of adamantane chloride was dropwise added in the above solution and then stirred another 12 h. After removed the solvent, the crude product was purified by dissolving in 5

DOI: 10.1021/acsami.5b04031
ACS Appl. Mater. Interfaces 2015, 7, 17171−17180

mL of dichloromethane and then washing with DI water three times. The organic phases were collected and dried overnight by $MgSO_4$, filtered, and evaporated to obtain 0.4 g of AD-NH-NH_2. As shown in Figure S2B, the ^{1}H NMR spectrum indicated the AD-NH-NH_2 was successfully prepared.

To synthesize AD-Hyd-DOX, AD-NH-NH_2 (134 mg) and doxorubicin hydrochloride (100 mg) were dissolved in 50 mL of dry methanol. Then, trifluoroacetic acid (50 μL) was added as a catalyst. The mixture was refluxed at 50 °C for 2 days in dark. Finally, the solution was concentrated by rotary evaporation and precipitated in ethyl acetate three times. The product was collected by centrifugation and dried under vacuum to obtain red AD-Hyd-DOX (102.5 mg). The molecular weight of AD-Hyd-DOX was determined by ESI-MS (Finnigan LCQadvantage). The calculated molecular mass of AD-Hyd-DOX was 719.3, and the ESI-MS result found to be 720.2 (Figure S3). As shown in Figure S2A and Figure S9, the ^{1}H NMR spectrum and ^{13}C NMR spectrum indicated that AD-Hyd-DOX was successfully prepared. ^{1}H NMR (DMSO-d_6, 300 MHz, Figure S2A) δ 0.79−0.90 ppm (s, 3H), 1.08−1.51 ppm (m, 8H), 1.58−2.02 ppm (m, 12H), 3.93−4.05 ppm (s, 3H), 4.11−4.25 ppm (s, 2H), 4.48−4.64 ppm (s, 2H), 4.88−5.16 ppm (m, 3H), 5.20−5.35 ppm (s, 1H), 5.42−5.52 ppm (s, 1H), 6.25−6.39 ppm (s, 1H), 7.58−7.98 ppm (m, 5H). ^{13}C NMR (DMSO-d_6, 300 MHz, Figure S9) δ 14.3 ppm, 17.3 ppm, 21.3 ppm, 27.8 ppm, 35.2 ppm, 36.2 ppm, 47.2 ppm, 57.0 ppm, 58.6 ppm, 66.7 ppm, 72.3 ppm, 77.9 ppm, 99.8 ppm, 110.7 ppm, 116.4 ppm, 120.2 ppm, 135.1 ppm, 136.8 ppm, 154.8 ppm, 158.2 ppm, 161.2 ppm, 186.3 ppm. In the ^{1}H NMR spectrum of AD-Hyd-DOX, the characteristic signals at δ 7.25 ppm belonging to −NH_2 in the AD-NH-NH_2 (Figure S2B) disappeared, and the proton signal of AD located at δ 1.5−2.0 ppm of AD-Hyd-DOX enhanced significantly, indicating the conjugation of AD-NH-NH_2 onto DOX. This was reconfirmed by the ^{13}C NMR spectrum, showing the signals (δ < 40 ppm) attributed to AD. These results confirmed that AD-Hyd-DOX have been prepared successfully.

2.4. Synthesis of Lipoic Acid Modified β-CD. According to previous literature procedure,[38] the lipoic acid modified β-CD was prepared with some minor modifications. In brief, 0.33 g of mono-6-ethylenediamine-β-CD was added to a solution of DMF containing lipoic acid (0.35 g), PyBOP (0.85 g), and DIEA (0.42 mL). The mixed solution was stirred for 1 day at the room temperature in a nitrogen round-bottom flask. Then the solution was concentrated and evaporated under reduced pressure. The residue was precipitated in acetone. After filtration, the product was collected and vacuum-dried. Then the product was dissolved in distilled water and freeze-dried. The molecular weight of the lipoic acid modified β-CD was determined by ESI-MS (Finnigan LCQadvantage). As displayed in Figure S6, the calculated molecular mass of the one lipoic acid molecule modified β-CD was 1365.3, and the ESI-MS result was found to be 1366.3. The calculated molecular mass of the two lipoic acid molecules modified β-CD was 1553.6.3 and the ESI-MS result was found to be 1554.7. As shown in Figure S4 and Figure S10, the ^{1}H NMR spectrum and ^{13}C NMR spectrum indicated the lipoic acid modified β-CD was successfully prepared. ^{1}H NMR (DMSO-d_6, 300 MHz, Figure S4) δ 0.76−1.92 ppm (m, 8H), 1.97−2.75 ppm (m, 5H), 2.98−3.73 ppm (m, 42H), 4.47−4.94 ppm (m, 14H), 5.65−5.89 ppm (m, 7H). ^{13}C NMR (DMSO-d_6, 300 MHz, Figure S10) δ 23.9 ppm, 24.9 ppm, 26.2 ppm, 28.2 ppm, 34.6 ppm, 35.9 ppm, 38.2 ppm, 46.6 ppm, 57.6 ppm, 60.3 ppm, 72.9 ppm, 73.7 ppm, 82.0 ppm, 102.0 ppm, 110.0 ppm, 118.1 ppm, 123.7 ppm, 172.9 ppm. In the ^{1}H NMR spectrum, the characteristic signals at δ 0.76−1.92 ppm belonging to lipoic acid were clearly detectable, indicating the conjugation of lipoic acid onto β-CD. This was also reconfirmed by the ^{13}C NMR spectrum, showing the signals at δ 23.9 ppm, 24.9 ppm, 26.2 ppm, 28.2 ppm, 34.6, 35.9, and 38.2 ppm attributed to the lipoic acid. This evidence indicated that lipoic acid have been conjugated with β-CD successfully.

2.5. Synthesis of β-Cyclodextrin-Modified Gold Nanoparticles (AuNP@CD). In brief, 60 mL of DMSO solution containing $HAuCl_4.3H_2O$ (150 mg) was quickly added into the mixed solution with 60 mL of DMSO containting 65 mg of lipoic acid modified β-CD and 240 mg of $NaBH_4$. The solution changed deep brown immediately and was stirred another 24 h at room temperature. Then 60 mL of CH_3CN was added to result in a black precipitate. The product was collected by centrifugation (12000× r, 20 min), washed with 60 mL of CH_3CN:DMSO (V:V = 1:1) and 60 mL of ethanol, and dried under vacuum overnight.

2.6. Preparation of the Multifunctional Nanocomposite AuNP@CD-AD-DOX/RGD. Due to the strong host−guest interaction between AD and β-CD, the peptide derivative AD-PEG_8-GRGDS and AD-Hyd-DOX were easily conjugated on the surface of AuNP@CD to form the multifunctional nanocomposite AuNP@CD-AD-DOX/RGD. To select optimal feed ratio, the concentration of the AD-Hyd-DOX was fixed at 5 μM and then increased the concentration of AuNPs from 1 to 15 μg/mL in the complex solution. After stirring 24 h at the room temperature, the fluorescence intensity of AD-Hyd-DOX was measured and observed that the fluorescence of AD-Hyd-DOX was completely quenched by AuNPs at 15 μg/mL. Therefore, in the progress of preparing AuNP@CD-AD-DOX/RGD, to ensure the fluorescence of AD-Hyd-DOX completely quenched by AuNPs, we preferentially conjugated the AD-Hyd-DOX (5 μM) with AuNPs (20 μg/mL) before adding excess AD-PEG_8-GRGDS (1 μM) to modify the AuNP@CD. All of the reactions were done under the nitrogen atmosphere and in the dark. After the complete of reactions, the complex solution was dialysized (MWCO: 3500 Da) against DI water for 2 days and lyophilized; then the functional AuNP@CD-AD-DOX/RGD was prepared. Moreover, through the fluorescence spectra standard curves of AD-Hyd-DOX, the amount of DOX loaded on AuNP@CD-AD-DOX/RGD was 10.8 wt % as analyzed by RF-530/PC spectrofluorophotometer after digesting AuNP@CD-AD-DOX/RGD by aqua regia. To examine the stability of DOX in aqua regia, the free DOX was treated with different amount of aqua regia, and then the fluorescence of DOX was detected by RF-530/PC spectrofluorophotometer. Specifically, 10 μL (0.1 mg/mL) free DOX solutions were added: 0, 10, 20, 30, 40, and 50 μL freshly prepared aqua regia, respectively. Then the mixtures were diluted to 1 mL by adding DI water and analyzed by RF-530/PC spectrofluorophotometer. As shown in Figure S11, the fluorescence of DOX almost unchanged in the presence of aqua regia, indicating that DOX was stable in the presence of aqua regia.

2.7. Characterization of AuNP@CD and AuNP@CD-AD-DOX/RGD. UV−vis spectrophotometer (Lambda Bio40, PerkinElmer) and RF-530/PC spectrofluorophotometer (Shimadzu) were employed to monitor the reaction process of preparing AuNP@CD-AD-DOX/RGD. Morphologies of AuNP@CD and AuNP@CD-AD-DOX/RGD were observed by transmission electronic microscopy (TEM, JEOL-2100).

2.8. Study of the Fluorescence of AuNP@CD-AD-DOX/RGD Recovered by Acid Stimulation. To study the fluorescence recovery of AuNP@CD-AD-DOX/RGD upon the acid stimulation, AuNP@CD-AD-DOX/RGD was incubated with pH 5.0 acetate buffer and pH 7.4 PBS buffer, respectively. The fluorescence of released DOX was monitored by RF-530/PC spectrofluorophotometer (Shimadzu) at given time intervals. The emission and excitation slit widths were set at 5 nm with λ_{ex} = 480 nm. To directly observe the recovered fluorescence of DOX, the Photographs were taken under white-light or illumination by an UV lamp.

2.9. Cell Culture. U87 cancer cells (Human glioblastoma cells) and COS7 normal cells (African green monkey kidney fibroblast cells) were incubated in DMEM medium with 10% FBS and 1% antibiotics (penicillin-streptomycin, 10000 U/mL) at 37 °C in a humidified atmosphere containing 5% CO_2.

2.10. Studying the Cancer-Targeted Ability of AuNP@CD-AD-DOX/RGD. U87 cancer cells and COS7 normal cells were seeded respectively in a glass bottom dish at a density of 1 × 10^5 cells/well for 24 h. As the negative control, U87 cells and COS7 cells were incubated with excess free RGD peptide (50 μM) for 4 h in advance. Thereafter, AuNP@CD-AD-DOX/RGD (containing 2 μg of DOX) dispersed in DMEM containing 10% FBS and 1% antibiotics were added, and the cells were incubated at 37 °C for another 3 or 6 h. After removing the medium and washing with PBS three times, the nuclei were stained

DOI: 10.1021/acsami.5b04031
ACS Appl. Mater. Interfaces 2015, 7, 17171−17180

with Hoechst 33342 at 37 °C for 15 min. Then the cells were observed by confocal laser scanning microscopy.

2.11. Quantitative Analysis of Cellular Uptake DOX by Flow Cytometry Assay. U87 cancer cells and COS7 normal cells were seeded in 24-well plates at a density of 5×10^4 cells/well and cultured with 1 mL of DMEM containing 10% FBS for 1 day. As the negative control, U87 and COS7 cells were incubated with excess free RGD peptide (50 μM) 4 h in advance. Then all cells were treated with AuNP@CD-AD-DOX/RGD (containing 2 μg of DOX) for another 3 or 6 h. After that, the medium was removed, and the cells were washed three times with PBS. Then all the cells were digested by trypsin and collected in centrifuge tubes by centrifugating at 1200 rpm for 3 min. The supernatant was discarded, and the cells were washed with PBS three times to remove excess AuNP@CD-AD-DOX/RGD. Then the suspended cells were filtrated and detected for red fluorescence of DOX (PE-A) by flow cytometry (BD FACSAria TM III, USA). Cells without AuNP@CD-AD-DOX/RGD treatment were used as the negative control. The fluorescence scan was performed with 1×10^4 cells.

2.12. Quantitative Evaluation of Intracellular Uptake Gold Content by ICP-MS Assay. To quantitatively detect the intracellular gold content, U87 cancer cells and COS7 normal cells were incubated with AuNP@CD-AD-DOX/RGD (containing 2 μg of DOX) for 3 and 6 h, respectively. To examine the blocking function of free RGD peptide, U87 cancer cells were incubated with excess free RGD peptide (50 μM) for 4 h in advance. After washed by PBS three times, the cells were counted and collected for ICP-MS analysis (model Agilent 7500a, Hewlett-Packard, Japan). Then the cell samples were digested by aqua regia, and each samples were coincubated with H_2O_2 (2 mL 30%, w/w) at 150 °C for 3 h. After the solution volume diluted with water to 10 mL, the gold content was analyzed by ICP-MS. The cells without treatment were used as the negative control.

2.13. Investigation of the Intracellular Drug Release Mechanism by Confocal Laser Scanning Microscopy. U87 cancer cells were seeded in a glass bottom dish at a density of 1×10^5 cells/well and cultured with 1 mL of DMEM containing 10% FBS for 1 day. Then the cells were treated with AuNP@CD-AD-DOX/RGD (containing 2 μg of DOX) for 12 or 24 h, respectively. Since the drug release is upon the acid condition of endo/lysosomes, we used NH_4Cl (20 mM) to block the acidification progression and neutralize the endo/lysosome pH. After that, the medium was removed, and the cells were washed three times with PBS. The nuclei were stained with Hoechst 33342 at 37 °C for 15 min. Then the cells were observed by confocal laser scanning microscopy.

Moreover, the release of anticancer drug DOX from lysosomes was examined by confocal laser scanning microscopy. When U87 cancer cells were incubated with AuNP@CD-AD-DOX/RGD (containing 2 μg of DOX) for 24 h in the presence of NH_4Cl (20 mM) or in the absence of NH_4Cl (20 mM), the cells were washed with PBS three times. Then the lysosomes were stained by LysoTracker Green DND-26 for 30 min and the nuclei were stained with Hoechst 33342 for 15 min. After these treatments, the cells were observed by confocal laser scanning microscopy. As shown in Figure S12, when the cells without NH_4Cl treatment, the red fluorescence of DOX was mainly detected at nuclei (Figure S12B1) since the DOX quickly escaped from the endo/lysosomes via free diffusion and entered the cell nuclei. However, the DOX was mainly observed in the lysosomes (Figure S12A3) in the presence of NH_4Cl treatment, whereas the green fluorescence of lysosomes has not changed (Figure S12B2 compared to Figure S12A2). These results indicated that DOX was released from the lysosomal compartment without the damage of lysosomes, which was the typical free diffusion process not due to the lysosome membranes disrupted by gold nanoparticles. Furthermore, the endo/lysosomal pH acidification protocol was performed by acridine orange staining according to the literature.[39] Briefly, U87 cancer cells were seeded in a glass bottom dish at a density of 1×10^5 cells/well and cultured with 1 mL of DMEM containing 10% FBS for 1 day. Then the cells were treated with NH_4Cl (20 mM) to block the acidification progression and neutralize the endo/lysosome pH. The cells without treament were as the control. Then all of the cells were stained by acridine orange (1 μg/mL) for 10 min, then washed with PBS for three times, and finally observed by confocal laser scanning microscopy. In term of acridine orange staining assay, red fluorescence was stained with acidic organelles, whereas green fluorescence was associated with high pH. As shown in Figure S13, when U87 cancer cells were treated with NH_4Cl (20 mM), the red fluorescence decreased remarkably, while the green fluorescence increased significantly. These results indicated that NH_4Cl could neutralize the endo/lysosomes pH and delay the endo/lysosomal acidification progress.

2.14. Observing Intracellular Distribution of AuNP@CD-AD-DOX/RGD by TEM. U87 cancer cells and COS7 normal cells were treated with AuNP@CD-AD-DOX/RGD (containing 2 μg of DOX) for 24 h. To examine the blocking function of free RGD peptide, U87 cancer cells were incubated with excess free RGD peptide (50 μM) for 4 h in advance. Then all cells were washed with PBS three times, collected, and fixed with 1 mL general fixative (containing 2.5% glutaraldehyde in 0.1 M PBS) at 4 °C and overnight. Cell samples were prepared for TEM observation according to standard procedures and then observed by electronic microscopy (TEM, JEOL-2100).

2.15. Evaluation of Therapeutic Effect of AuNP@CD-AD-DOX/RGD in Vitro. In vitro cytotoxicity was performed with U87 cancer cells and COS7 normal cells by MTT assay. Briefly, U87 and COS7 cells were seeded in 96-well plates at a density of 6000 cells/well, and then the cells were incubated in 100 μL of DMEM containing 10% FBS and 1% antibiotics for 1 day prior to adding AuNP@CD-AD-DOX/RGD with or without the addition of NH_4Cl (20 mM). After coincubation for 2 days, the medium was replaced with 200 μL of fresh medium. Then 20 μL MTT solutions (5 mg/mL) was added to each well and further incubated for 4 h. After that, the medium was removed, and 200 μL of DMSO was added. The absorbance was measured at 570 nm using a microplate reader (Bio-Rad, model 550, USA). The relative cell viability was calculated as cell viability = $(OD_{570\ (samples)}/OD_{570\ (control)}) \times 100\%$, where $OD_{570\ (control)}$ was obtained in the absence of AuNP@CD-AD-DOX/RGD with or without the addition of NH_4Cl (20 mM), and $OD_{570\ (samples)}$ was obtained in the presence of AuNP@CD-AD-DOX/RGD with or without the addition of NH_4Cl (20 mM). Each value was averaged from four independent experiments.

2.16. Statistics Analysis. The quantitative data collected were expressed as mean ± SD. Statistical significance was analyzed by Student's test. The statistical significance was inferred at a value of $P < 0.05$.

3. RESULTS AND DISCUSSION

3.1. Preparation and Characterization of the Multifunctional Nanocomposite. In this study, the β-cyclodextrin-modified gold nanoparticles were synthesized via the classical $NaBH_4$ reduction method according to the reported protocol.[38,40] As displayed in Figure S5, the simple AuNP@CD showed the favorable monodispersion and uniform spherical shape as an individual nanoparticle. Due to the strong host−guest interaction between β-CD and AD, AD-PEG_8-GRGDS and AD-Hyd-DOX were conveniently assembled on the surface of AuNP@CD. As shown in Figure 1A and B, the multifunctional AuNP@CD-AD-DOX/RGD also dispersed well and had the narrow size distribution with the mean diameter of about 3.3 nm. UV−visible spectroscopy presented in Figure 1C indicated that AuNP@CD-AD-DOX/RGD was stable in aqueous solution, and no aggregation occurred after the surface incorporation of AD-PEG_8-GRGDS and AD-Hyd-DOX.

Moreover, it is well-known that gold nanoparticles have been served as ultraefficient quenchers of a chromophore when modified on the surface of AuNPs.[41−43] When AD-Hyd-DOX conjugated on the surface of gold nanoparticles via host−guest interaction, the fluorescence of AD-Hyd-DOX was quenched by AuNP@CD as expected. As shown in Figure 2A, the

DOI: 10.1021/acsami.5b04031
ACS Appl. Mater. Interfaces 2015, 7, 17171−17180

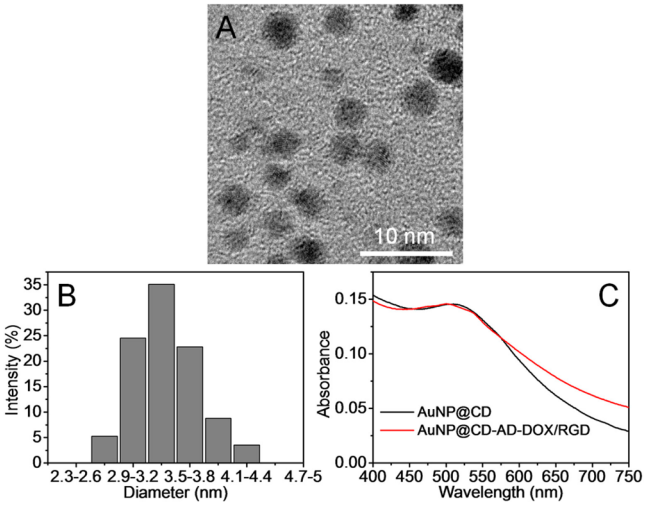

Figure 1. Characterizations of the multifunctional nanocomposite AuNP@CD-AD-DOX/RGD by transmission electron microscopy (TEM) and UV−visible spectroscopy. (A) TEM image of AuNP@CD-AD-DOX/RGD. (B) Size distribution of AuNP@CD-AD-DOX/RGD. (C) Normalized UV−visible spectroscopy of AuNP@CD and AuNP@CD-AD-DOX/RGD.

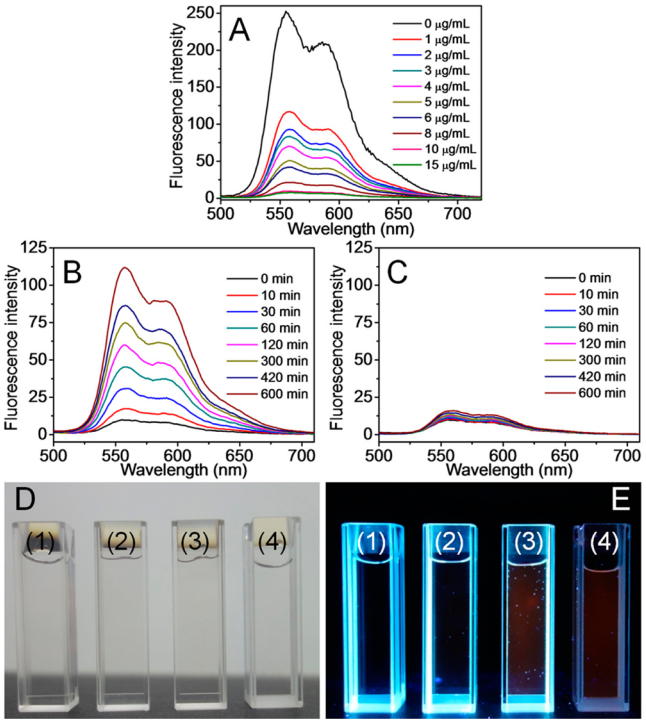

Figure 2. Evaluation of the fluorescence quenching ability of AuNP@CD and investigation of the acid-sensitive of AuNP@CD-AD-DOX/RGD. (A) Fluorescence emission spectra of AD-Hyd-DOX (5 μM) with the addition of different amounts of AuNP@CD. Fluorescence emission spectra of AuNP@CD-AD-DOX/RGD upon incubating in pH 5.0 acetate buffer (B) and pH 7.4 PBS buffer (C) for different periods. (D) Photograph taken under white light and (E) photograph taken under illumination by an UV lamp. From left to right are (1) the pure AuNP@CD; (2) AuNP@CD-AD-DOX/RGD incubated in pH 7.4 PBS buffer for 1 h; (3) AuNP@CD-AD-DOX/RGD incubated in pH 5.0 acetate buffer for 1 h, and (4) free DOX solution.

fluorescence intensity of AD-Hyd-DOX decreased markedly when gradually increased AuNP@CD concentration from 1 to 15 μg/mL, and the calculated maximum quenching efficacy of AuNP@CD was 97.2 ± 0.2%. The quenched fluorescence can be recovered under the trigger of acid stimulation, which contributed to monitor the intracellular release of drug. As the smart drug nanocarrier, AuNP@CD-AD-DOX/RGD was able to release DOX quickly upon the trigger of acid microenvironment of endo/lysosomes. As shown in Figure 2B, when AuNP@CD-AD-DOX/RGD was incubated with the pH 5.0 buffer, the fluorescence of DOX enhanced significantly and increased with the prolonging time. Upon treating with the acid stimulus, the hydrazone linkage between AD and DOX would be cleaved and triggered the release of DOX, resulting in disappearance of the nanosurface fluorescence energy resonance transfer (FRET) effect between AuNP@CD and DOX.[44] Synchronously, the fluorescence of DOX was recovered, which can be further used to track the intracellular drug release. In contrast, at the normal physiological pH, there was negligible fluorescence recovered (Figure 2C), and nearly no DOX was released since the hydrazone bond was stable at pH 7.4. To directly observe the drug release from AuNP@CD-AD-DOX/RGD upon the trigger of intracellular acid microenvironment of endo/lysosomes, the red fluorescence of AuNP@CD-AD-DOX/RGD was detected after incubating with the pH 5.0 buffer for 1 h. As shown in Figure 2D and E, the remarkable red fluorescence of DOX was observed at the acid condition, but the negligible fluorescence was found at the normal physiological pH. These results demonstrated that AuNP@CD-AD-DOX/RGD was stable at normal physiological conditions and could rapidly respond to intracellular acid microenvironment to trigger intracellular drug release for cancer treatment.

3.2. Cancer-Targeted Internalization and Intracellular Drug Release of AuNP@CD-AD-DOX/RGD. Cancer-targeted drug delivery contributes to selectively destroy cancer cells and reduce adverse effects to normal cells. To confirm the specific selectivity of the multifunctional nanocomposite, U87 cancer cells (Human glioblastoma cells) with overexpressed $\alpha_v\beta_3$ integrin receptor on the cell membrane and $\alpha_v\beta_3$ integrin receptor-negative COS7 normal cells (African green monkey kidney fibroblast cells) were chosen to coincubate with AuNP@CD-AD-DOX/RGD, respectively. As shown in Figure 3, the significant red fluorescence of DOX was observed in U87 cancer cells, and the red fluorescence enhanced with increasing incubation time. However, in COS7 normal cells, only weak red fluorescence was detected (Figure 3D−F). With the aid of RGD peptide moiety, AuNP@CD-AD-DOX/RGD could actively target to cancer cells and increase the cellular uptake via receptor-mediated endocytosis. However, when the $\alpha_v\beta_3$ integrin was blocked by free RGD peptide in advance, the cellular uptake would be remarkably inhibited (Figure 3C), which confirmed that the selective uptake of AuNP@CD-AD-DOX/RGD was owing to the active targeting ability of RGD. Furthermore, flow cytometry analysis was employed to evaluate the intracellular fluorescence intensity of DOX quantitatively. As indicated in Figure 4A and B, the cellular content of anticancer drug DOX in U87 cancer cells was more than that in COS7 normal cells at each time point, and stronger fluorescence was observed in U87 cells. If the $\alpha_v\beta_3$ integrin was blocked by excess free RGD peptide, the cellular internalization of DOX was dramatically decreased in U87 cancer cells. Semiquantitative fluorescence intensity analysis also confirmed that mean integrated photoluminescence intensity of DOX in U87 cancer cells were 2.4- and 3.5-fold

DOI: 10.1021/acsami.5b04031
ACS Appl. Mater. Interfaces 2015, 7, 17171−17180

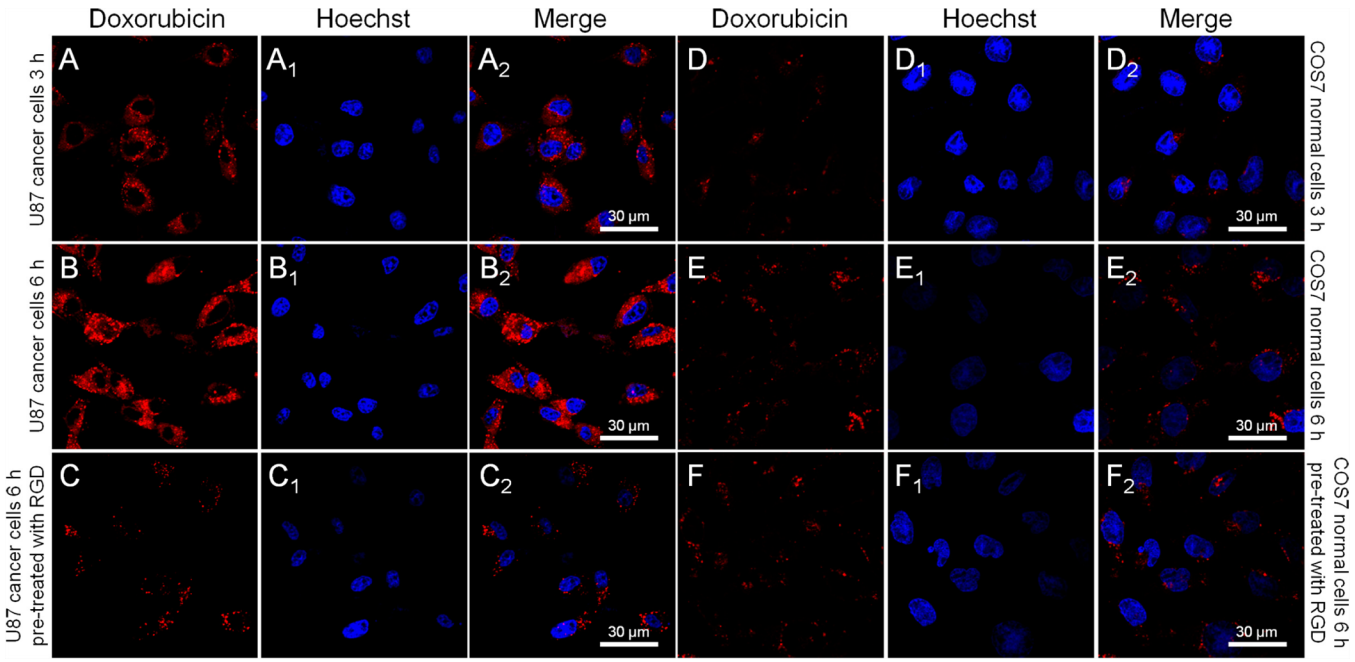

Figure 3. Evaluation of the cancer-targeted uptake ability of AuNP@CD-AD-DOX/RGD. Confocal laser scanning microscopy (CLSM) images of U87 cancer cells incubated with AuNP@CD-AD-DOX/RGD for 3 h (A–A_2), 6 h (B–B_2), and 6 h for U87 cancer cells pretreated with excess free RGD peptide in advance (C–C_2). And CLSM images of COS7 normal cells incubated with AuNP@CD-AD-DOX/RGD for 3 h (D–D_2), 6 h (E–E_2), and 6 h for COS7 normal cells pretreated with the excess of free RGD peptide in advance (F–F_2). (A–F) red fluorescence images of doxorubicin; (A_1–F_1) blue fluorescence images of nuclei; (A_2–F_2) the merged images of red and blue fluorescences.

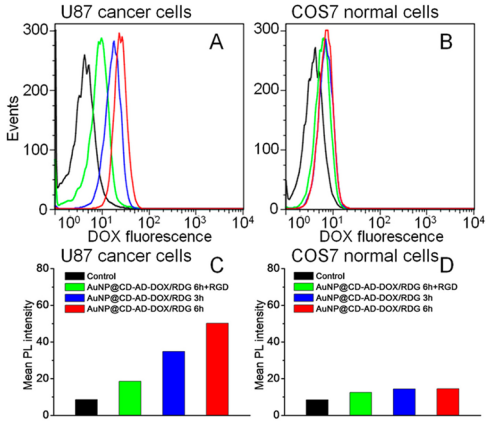

Figure 4. Quantitative flow cytometry analysis of the cellular DOX red fluorescence in U87 cancer cells (A) and COS7 normal cells (B). The cells without treatment (blank line), treated with AuNP@CD-AD-DOX/RGD for 3 h (blue line), 6 h (red line), and 6 h (green line) for cells pretreated with excess free RGD peptide in advance, respectively. The mean integrated photoluminescence (PL) intensity of DOX in U87 cancer cells (C) and COS7 normal cells (D) at different incubation conditions.

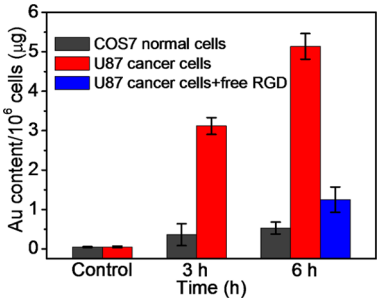

Figure 5. Quantitative analysis of gold content by ICP-MS in U87 cancer cells and COS7 normal cells treated with AuNP@CD-AD-DOX/RGD 3 and 6 h, respectively. To examine the blocking function of free RGD peptide, U87 cancer cells were incubated with the excess free RGD peptide (50 μM) for 4 h in advance. The cells without treatment were used as a negative control.

higher than that of COS7 normal cells when incubated with AuNP@CD-AD-DOX/RGD for 3 or 6 h, respectively (Figure 4C and D). These results confirmed that AuNP@CD-AD-DOX/RGD has strong ability to promote the cellular uptake in cancer cells with the overexpressed $\alpha_v\beta_3$ integrin receptor. Furthermore, the gold content of cells incubated with AuNP@CD-AD-DOX/RGD was examined quantitatively by using inductively coupled plasma-mass spectrometry (ICP-MS). As shown in Figure 5, the internalized gold content increased remarkably with the prolonged incubation time of U87 cancer cells. In contrast, there was only a little gold was uptaken by COS7 normal cells. When coincubated with AuNP@CD-AD-DOX/RGD, the uptake content of gold in U87 cells was 8.6-fold and 9.5-fold higher than that in COS7 cells, which was consistent with CLSM observations. Moreover, when the $\alpha_v\beta_3$ integrin was blocked by excess RGD peptide in advance, the cellular internalization of gold was dramatically decreased in U87 cancer cells.

3.3. Study on Intracellular Drug Release Mechanism of AuNP@CD-AD-DOX/RGD. It is well-known that efficient intracellular delivery of anticancer drug into the target organelle could potentiate the therapeutic effect. Therefore, to achieve satisfactory therapeutic effect, it is critically important to efficiently deliver the active anticancer drug to final target destination where drugs exert the functions. As the promising candidate of drug carrier, ultrasmall (2–4 nm) gold nanoparticles have demonstrated unique advantages to penetrate cancer cells and achieve high accumulation in the tumor site for

DOI: 10.1021/acsami.5b04031
ACS Appl. Mater. Interfaces 2015, 7, 17171–17180

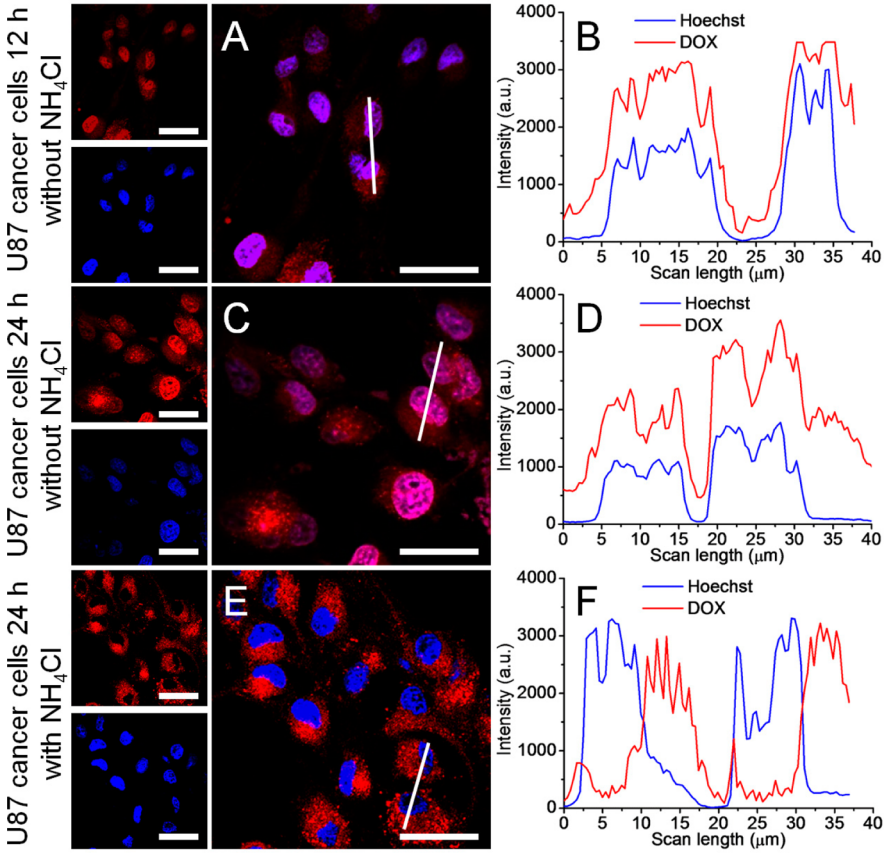

Figure 6. Study on the intracellular drug release mechanism of AuNP@CD-AD-DOX/RGD. CLSM images of U87 cancer cells incubated with AuNP@CD-AD-DOX/RGD for 12 h (A), 24 h (C), and 24 h (E) in the presence of NH_4Cl (20 mM). B, D, and F are the line-scan profiles of fluorescence intensity from A, C, and E, respectively. The blue and red curves in the line-scan profiles represent the fluorescence intensities from Hoechst and DOX, respectively. The scale bars are 30 μm.

targeted therapy.[8,45,46] As shown in Figure 6, when U87 cancer cells were treated with AuNP@CD-AD-DOX/RGD for 12 and 24 h, the red fluorescence of DOX was detected in the nucleus and exhibited favorable overlap with the Hoechst-stained nuclei. After the specific uptake by cancer cells, DOX was rapidly liberated from AuNP@CD-AD-DOX/RGD since the hydrazone bond was destructed by the acidic endo/lysosomes and subsequently diffused to the nuclei. It has been reported that the NH_4Cl treatment could increase the pH of endo/lysosomes and inhibit the acidification of endo/lysosomes.[47,48] To determine this controllable drug release mechanism, NH_4Cl was introduced to neutralize the endo/lysosomes pH and inhibit the release of drug.[49] As shown in Figure 6E and F, when treated with NH_4Cl, the majority of red fluorescence from DOX was observed in the cytoplasm, and very little red fluorescence distributed in the nucleus. In the NH_4Cl-treated cells, the endo/lysosome acidification was blocked to some extent, leading to the delay of the DOX release and thereafter impeding the diffusion of anticancer drug into the nucleus. The NH_4Cl treatment confirmed that the acidifying intracellular microenvironment was beneficial for AuNP@CD-AD-DOX/RGD to trigger drug release for cancer therapy. It is well-known that DOX has been demonstrated to be stable in the lysosomal compartments,[50] which is favorable for developing the intelligent drug delivery system to respond the acidic lysosomal microenvironment for intracellular drug release.

To precisely detect the intracellular localization of AuNP@CD-AD-DOX/RGD nanocomposite, the cells treated with AuNP@CD-AD-DOX/RGD were analyzed by transmission electron microscope (TEM). As shown in Figure 7A, the uptake of AuNP@CD-AD-DOX/RGD in U87 cancer cells was much more than that in COS7 normal cells (Figure 7E), indicating that the nanocomposites were quickly endocytosed by cancer cells. This was due to the active targeting ability of RGD peptide in nanocomposite, which selectively improved the uptake of cancer cells via the receptor-mediated endocytosis. The internalization of AuNP@CD-AD-DOX/RGD was significantly reduced when the cells were pretreated with excess free RGD peptide in advance (Figure 7C). Since the $\alpha_v\beta_3$ integrin integrated with free RGD, the internalization of AuNP@CD-AD-DOX/RGD was inhibited.

3.4. Study of the Anticancer Effect of AuNP@CD-AD-DOX/RGD in Vitro. In order to investigate the anticancer effect of multifunctional nanocomposite AuNP@CD-AD-DOX/RGD, the cell cytotoxicity was evaluated by 3-[4,5-dimethylthiazol-2-yl]-2,5-diphenyltetra-zolium bromide (MTT) assay. As displayed in Figure 8, the cell viability of U87 cancer cells decreased dramatically to 30% when treated with AuNP@CD-AD-DOX/RGD for 48 h. However, the COS7 normal cell viability was more than 70%. Obviously, the growth of U87 cancer cells was selectively inhibited by the multifunctional nanocomposite. The specific targeting ability of AuNP@CD-AD-DOX/RGD promoted the increased uptake of cancer cells and subsequent intracellular release of anticancer drug potentiated the therapeutic effect, inducing the death of cancer cells. As expected, when the way of intracellular drug release

DOI: 10.1021/acsami.5b04031
ACS Appl. Mater. Interfaces 2015, 7, 17171−17180

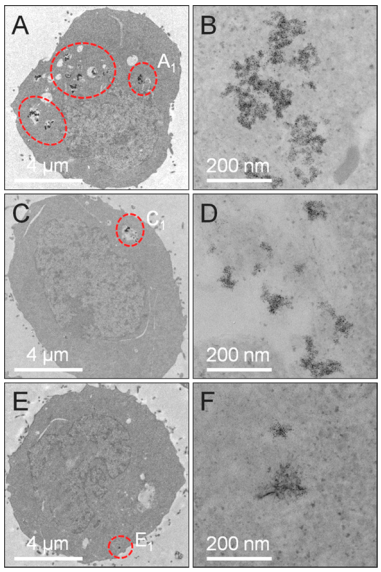

Figure 7. Evaluating the intracellular distribution of AuNP@CD-AD-DOX/RGD by TEM observation. (A) Representative TEM image of U87 cancer cells incubated with AuNP@CD-AD-DOX/RGD for 24 h. (B) The enlarged TEM image from the circled area in (A_1). (C) TEM image of U87 cancer cells incubated with AuNP@CD-AD-DOX/RGD for 24 h and the cells pretreated with excess free RGD peptide in advance. (D) Enlarged TEM image from the circled area in C_1. (E) TEM image of COS7 normal cells incubated with AuNP@CD-AD-DOX/RGD 24 h. (F) Enlarged TEM image from the circled area in E_1.

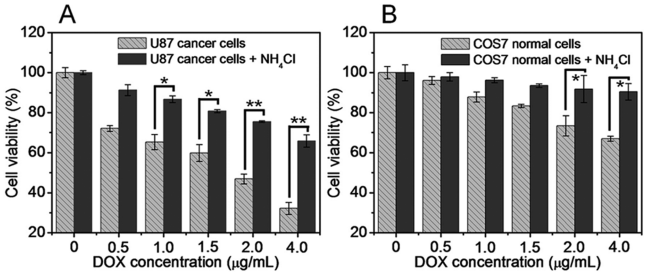

Figure 8. Study the anticancer effect of AuNP@CD-AD-DOX/RGD in vitro. The cell viability of U87 cancer cells (A) and COS7 normal cells (B) after incubated with the multifunctional nanocomposite AuNP@CD-AD-DOX/RGD in the absence or in the presence of NH_4Cl (20 mM) for 48 h. The statistical significance in difference was analyzed using student's *T*-test: $*p < 0.05$ and $**p < 0.01$.

was blocked by NH_4Cl treatment, the cell cytotoxicity reduced markedly, especially at the high DOX concentrations of 2.0 and 4.0 μg/mL. These results confirmed that the active targeting and controllable cellular release ability of drug carrier was beneficial to eliminate cancer cells specifically and reduce the damage to normal cells.

4. CONCLUSION

In summary, a versatile gold nanoparticle-based multifunctional nanocomposite AuNP@CD-AD-DOX/RGD was constructed via host−guest interaction for targeted cancer chemotherapy. The RGD peptide moiety could increase cancer cell uptake via the receptor-mediated endocytosis, and then the anticancer drug was triggered release by the intrinsic acid condition of endo/lysosomes in cancer cells, inducing the significantly enhanced cell growth inhibition for cancer cells. The construction of multifunctional AuNPs by host−guest interaction for targeted cancer therapy with reduced side effect opens a window of designing versatile multifunctional drug delivery systems, which have great potential in cancer therapy.

■ ASSOCIATED CONTENT

Supporting Information

The Supporting Information is available free of charge on the ACS Publications website at DOI: 10.1021/acsami.5b04031.

ESI-MS profile of the peptide AD-PEG_8-GRGDS, the prodrug AD-Hyd-DOX and lipoic acid modified β-CD; the ^1H NMR spectra of AD-Hyd-DOX, AD-NH-NH_2, and lipoic acid modified β-CD; the ^{13}C NMR spectra of AD-Hyd-DOX, AD-NH-NH_2, and lipoic acid modified β-CD; the TEM image of β-cyclodextrin-modified gold nanoparticle (AuNP@CD); the fluorescence spectra of DOX coincubate with aqua regia; the CLSM images of confirming the lysosomal DOX detection; the CLSM images of evaluating endo/lysosomal pH (PDF)

■ AUTHOR INFORMATION

Corresponding Author

*Tel.: + 86 27 6875 5993. Fax: + 86 27 6875 4509. E-mail address: xz-zhang@whu.edu.cn (X. Z. Zhang).

Notes

The authors declare no competing financial interest.

■ ACKNOWLEDGMENTS

This work was supported by the National Natural Science Foundation of China (51125014 and 51233003), the Ministry of Science and Technology of China (2011CB606202), the Ministry of Education of China (20120141130003), and supported by the Fundamental Research Funds for the Central Universities (2014203020201 and 2014203020204).

■ ABBREVIATIONS

AuNP, gold nanoparticle

AuNP@CD, β-cyclodextrin-modified gold nanoparticle

AD-PEG_8-GRGDS, the adamantane-PEG_8-glycine-arginine-glycine-aspartic-serine

AD-Hyd-DOX, the adamantane conjugated anticancer drug doxorubicin with hydrazone bond linkage

AuNP@CD-AD-DOX/RGD, AuNP@CD conjugated with AD-Hyd-DOX and AD-PEG_8-GRGDS via host−guest interaction

■ REFERENCES

(1) Zhang, L.; Gu, F. X.; Chan, J. M.; Wang, A. Z.; Langer, R. S.; Farokhzad, O. C. Nanoparticles in Medicine: Therapeutic Applications and Developments. *Clin. Pharmacol. Ther.* **2008**, *83*, 761−769.

(2) Sapsford, K. E.; Algar, W. R.; Berti, L.; Gemmill, K. B.; Casey, B. J.; Oh, E.; Stewart, M. H.; Medintz, I. L. Functionalizing Nanoparticles with Biological Molecules: Developing Chemistries That Facilitate Nanotechnology. *Chem. Rev.* **2013**, *113*, 1904−2074.

(3) Yang, F.; Jin, C.; Subedi, S.; Lee, C. L.; Wang, Q.; Jiang, Y.; Li, J.; Di, Y.; Fu, D. Emerging Inorganic Nanomaterials for Pancreatic Cancer Diagnosis and Treatment. *Cancer Treat. Rev.* **2012**, *38*, 566−579.

(4) Giljohann, D. A.; Seferos, D. S.; Daniel, W. L.; Massich, M. D.; Patel, P. C.; Mirkin, C. A. Gold Nanoparticles for Biology and Medicine. *Angew. Chem., Int. Ed.* **2010**, *49*, 3280−3294.

DOI: 10.1021/acsami.5b04031
ACS Appl. Mater. Interfaces 2015, 7, 17171−17180

(5) Bunz, U. H.; Rotello, V. M. Gold Nanoparticle-Fluorophore Complexes: Sensitive and Discerning "Noses" for Biosystems Sensing. *Angew. Chem., Int. Ed.* **2010**, *49*, 3268−3279.
(6) Weintraub, K. Biomedicine: The New Gold Standard. *Nature* **2013**, *495*, S14−S16.
(7) Choi, H. S.; Liu, W.; Misra, P.; Tanaka, E.; Zimmer, J. P.; Itty Ipe, B.; Bawendi, M. G.; Frangioni, J. V. Renal Clearance of Quantum Dots. *Nat. Biotechnol.* **2007**, *25*, 1165−1170.
(8) Huang, K.; Ma, H.; Liu, J.; Huo, S.; Kumar, A.; Wei, T.; Zhang, X.; Jin, S.; Gan, Y.; Wang, P. C.; He, S.; Zhang, X.; Liang, X. J. Size-Dependent Localization and Penetration of Ultrasmall Gold Nanoparticles in Cancer Cells, Multicellular Spheroids, and Tumors in Vivo. *ACS Nano* **2012**, *6*, 4483−4493.
(9) Liu, J.; Yu, M.; Zhou, C.; Yang, S.; Ning, X.; Zheng, J. Passive Tumor Targeting of Renal-Clearable Luminescent Gold Nanoparticles: Long Tumor Retention and Fast Normal Tissue Clearance. *J. Am. Chem. Soc.* **2013**, *135*, 4978−4981.
(10) Liu, J.; Yu, M.; Ning, X.; Zhou, C.; Yang, S.; Zheng, J. PEGylation and Zwitterionization: Pros and Cons in the Renal Clearance and Tumor Targeting of Near-IR-Emitting Gold Nanoparticles. *Angew. Chem., Int. Ed.* **2013**, *52*, 12572−12576.
(11) Nicolas, J.; Mura, S.; Brambilla, D.; Mackiewicz, N.; Couvreur, P. Design, Functionalization Strategies and Biomedical Applications of Targeted Biodegradable/Biocompatible Polymer-Based Nanocarriers for Drug Delivery. *Chem. Soc. Rev.* **2013**, *42*, 1147−1235.
(12) Mahmud, A.; Xiong, X. B.; Aliabadi, H. M.; Lavasanifar, A. Polymeric Micelles for Drug Targeting. *J. Drug Target* **2007**, *15*, 553−584.
(13) Zou, Y.; Song, Y.; Yang, W.; Meng, F.; Liu, H.; Zhong, Z. Galactose-Installed Photo-Crosslinked pH-Sensitive Degradable Micelles for Active Targeting Chemotherapy of Hepatocellular Carcinoma in Mice. *J. Controlled Release* **2014**, *193*, 154−161.
(14) Chen, W. H.; Xu, X. D.; Luo, G. F.; Jia, H. Z.; Lei, Q.; Cheng, S. X.; Zhuo, R. X.; Zhang, X. Z. Dual-Targeting Pro-Apoptotic Peptide for Programmed Cancer Cell Death via Specific Mitochondria Damage. *Sci. Rep.* **2013**, *3*, 3468.
(15) Dai, J.; Lin, S.; Cheng, D.; Zou, S.; Shuai, X. Interlayer-Crosslinked Micelle with Partially Hydrated Core Showing Reduction and pH Dual Sensitivity for Pinpointed Intracellular Drug Release. *Angew. Chem., Int. Ed.* **2011**, *50*, 9404−9408.
(16) Chu, Z.; Dreiss, C. A.; Feng, Y. Smart Wormlike Micelles. *Chem. Soc. Rev.* **2013**, *42*, 7174−7203.
(17) Nakayama, M.; Akimoto, J.; Okano, T. Polymeric Micelles with Stimuli-Triggering Systems for Advanced Cancer Drug Targeting. *J. Drug Target* **2014**, *22*, 584−599.
(18) Mura, S.; Nicolas, J.; Couvreur, P. Stimuli-Responsive Nanocarriers for Drug Delivery. *Nat. Mater.* **2013**, *12*, 991−1003.
(19) Wang, F.; Wang, Y. C.; Dou, S.; Xiong, M. H.; Sun, T. M.; Wang, J. Doxorubicin-Tethered Responsive Gold Nanoparticles Facilitate Intracellular Drug Delivery for Overcoming Multidrug Resistance in Cancer Cells. *ACS Nano* **2011**, *5*, 3679−3692.
(20) Zhan, F.; Chen, W.; Wang, Z.; Lu, W.; Cheng, R.; Deng, C.; Meng, F.; Liu, H.; Zhong, Z. Acid-Activatable Prodrug Nanogels for Efficient Intracellular Doxorubicin Release. *Biomacromolecules* **2011**, *12*, 3612−3620.
(21) Zhou, L.; Cheng, R.; Tao, H.; Ma, S.; Guo, W.; Meng, F.; Liu, H.; Liu, Z.; Zhong, Z. Endosomal pH-Activatable Poly(Ethylene Oxide)-Graft-Doxorubicin Prodrugs: Synthesis, Drug Release, and Biodistribution in Tumor-Bearing Mice. *Biomacromolecules* **2011**, *12*, 1460−1467.
(22) Song, L.; Ho, V. H.; Chen, C.; Yang, Z.; Liu, D.; Chen, R.; Zhou, D. Efficient, pH-Triggered Drug Delivery Using a pH-Responsive DNA-Conjugated Gold Nanoparticle. *Adv. Healthcare Mater.* **2013**, *2*, 275−280.
(23) Xu, X.; Li, Y.; Li, H.; Liu, R.; Sheng, M.; He, B.; Gu, Z. Smart Nanovehicles Based on pH-Triggered Disassembly of Supramolecular Peptide-Amphiphiles for Efficient Intracellular Drug Delivery. *Small* **2014**, *10*, 1133−1140.
(24) Ruan, S.; Cao, X.; Cun, X.; Hu, G.; Zhou, Y.; Zhang, Y.; Lu, L.; He, Q.; Gao, H. Matrix Metalloproteinase-Sensitive Size-Shrinkable Nanoparticles for Deep Tumor Penetration and pH Triggered Doxorubicin Release. *Biomaterials* **2015**, *60*, 100−110.
(25) Hu, Q. D.; Tang, G. P.; Chu, P. K. Cyclodextrin-Based Host-Guest Supramolecular Nanoparticles for Delivery: from Design to Applications. *Acc. Chem. Res.* **2014**, *47*, 2017−2025.
(26) Hu, J.; Liu, S. Engineering Responsive Polymer Building Blocks with Host-Guest Molecular Recognition for Functional Applications. *Acc. Chem. Res.* **2014**, *47*, 2084−2095.
(27) Kang, Y.; Guo, K.; Li, B. J.; Zhang, S. Nanoassemblies Driven by Cyclodextrin-Based Inclusion Complexation. *Chem. Commun.* **2014**, *50*, 11083−11092.
(28) Yu, G.; Jie, K.; Huang, F. Supramolecular Amphiphiles Based on Host-Guest Molecular Recognition Motifs. *Chem. Rev.* **2015**, DOI: 10.1021/cr5005315.
(29) Liu, K.; Kang, Y.; Wang, Z.; Zhang, X. 25th Anniversary Article: Reversible and Adaptive Functional Supramolecular Materials: "Noncovalent Interaction" Matters. *Adv. Mater.* **2013**, *25*, 5530−5548.
(30) Zhang, J.; Ma, P. X. Host-Guest Interactions Mediated Nano-Assemblies Using Cyclodextrin-Containing Hydrophilic Polymers and Their Biomedical Applications. *Nano Today* **2010**, *5*, 337−350.
(31) Shi, Y.; Goodisman, J.; Dabrowiak, J. C. Cyclodextrin Capped Gold Nanoparticles as a Delivery Vehicle for a Prodrug of Cisplatin. *Inorg. Chem.* **2013**, *52*, 9418−9426.
(32) Aykaç, A.; Martos-Maldonado, M. C.; Casas-Solvas, J. M.; Quesada-Soriano, I.; García-Maroto, F.; García-Fuentes, L.; Vargas-Berenguel, A. β-Cyclodextrin-Bearing Gold Glyconanoparticles for the Development of Site Specific Drug Delivery Systems. *Langmuir* **2014**, *30*, 234−242.
(33) Zitzmann, S.; Ehemann, V.; Schwab, M. Arginine-Glycine-Aspartic Acid (RGD)-Peptide Binds to Both Tumor and Tumor-Endothelial Cells in Vivo. *Cancer Res.* **2002**, *62*, 5139−5143.
(34) Luo, G. F.; Chen, W. H.; Liu, Y.; Zhang, J.; Cheng, S. X.; Zhuo, R. X.; Zhang, X. Z. Charge-Reversal Plug Gate Nanovalves on Peptide-Functionalized Mesoporous Silica Nanoparticles for Targeted Drug Delivery. *J. Mater. Chem. B* **2013**, *1*, 5723−5732.
(35) Luo, G. F.; Xu, X. D.; Zhang, J.; Yang, J.; Gong, Y. H.; Lei, Q.; Jia, H. Z.; Li, C.; Zhuo, R. X.; Zhang, X. Z. Encapsulation of an Adamantane-Doxorubicin Prodrug in pH-Responsive Polysaccharide Capsules for Controlled Release. *ACS Appl. Mater. Interfaces* **2012**, *4*, 5317−5324.
(36) Chen, W. H.; Xu, X. D.; Jia, H. Z.; Lei, Q.; Luo, G. F.; Cheng, S. X.; Zhuo, R. X.; Zhang, X. Z. Therapeutic Nanomedicine Based on Dual-Intelligent Functionalized Gold Nanoparticles for Cancer Imaging and Therapy in Vivo. *Biomaterials* **2013**, *34*, 8798−8807.
(37) Hassan, G. S.; El-Emam, A. A.; Gad, L. M.; Barghash, A. E. Synthesis, Antimicrobial and Antiviral Testing of Some New 1-Adamantyl Analogues. *Saudi Pharm. J.* **2010**, *18*, 123−128.
(38) Wang, H.; Chen, Y.; Li, X. Y.; Liu, Y. Synthesis of Oligo(Ethylenediamino)-beta-Cyclodextrin Modified Gold Nanoparticle as a DNA Concentrator. *Mol. Pharmaceutics* **2007**, *4*, 189−198.
(39) Salerno, M.; Avnet, S.; Bonuccelli, G.; Hosogi, S.; Granchi, D.; Baldini, N. Impairment of Lysosomal Activity as a Therapeutic Modality Targeting Cancer Stem Cells of Embryonal Rhabdomyosarcoma Cell Line RD. *PLoS One* **2014**, *9*, e110340.
(40) Li, N.; Chen, Y.; Zhang, Y. M.; Yang, Y.; Su, Y.; Chen, J. T.; Liu, Y. Polysaccharide-Gold Nanocluster Supramolecular Conjugates as a Versatile Platform for the Targeted Delivery of Anticancer Drugs. *Sci. Rep.* **2014**, *4*, 4164.
(41) Sapsford, K. E.; Berti, L.; Medintz, I. L. Materials for Fluorescence Resonance Energy Transfer Analysis: Beyond Traditional Donor-Acceptor Combinations. *Angew. Chem., Int. Ed.* **2006**, *45*, 4562−4589.
(42) Darbha, G. K.; Ray, A.; Ray, P. C. Gold Nanoparticle-Based Miniaturized Nanomaterial Surface Energy Transfer Probe for Rapid and Ultrasensitive Detection of Mercury in Soil, Water, and Fish. *ACS Nano* **2007**, *1*, 208−214.

DOI: 10.1021/acsami.5b04031
ACS Appl. Mater. Interfaces 2015, 7, 17171−17180

(43) Chen, W. H.; Luo, G. F.; Xu, X. D.; Jia, H. Z.; Lei, Q.; Han, K.; Zhang, X. Z. Cancer-Targeted Functional Gold Nanoparticles for Apoptosis Induction and Real-Time Imaging Based on FRET. *Nanoscale* **2014**, *6*, 9531−9535.
(44) Kim, D.; Jeong, Y. Y.; Jon, S. A Drug-Loaded Aptamer-Gold Nanoparticle Bioconjugate for Combined CT Imaging and Therapy of Prostate Cancer. *ACS Nano* **2010**, *4*, 3689−3696.
(45) Huo, S.; Jin, S.; Ma, X.; Xue, X.; Yang, K.; Kumar, A.; Wang, P. C.; Zhang, J.; Hu, Z.; Liang, X. J. Ultrasmall Gold Nanoparticles as Carriers for Nucleus-Based Gene Therapy due to Size-Dependent Nuclear Entry. *ACS Nano* **2014**, *8*, 5852−5862.
(46) Sousa, A. A.; Morgan, J. T.; Brown, P. H.; Adams, A.; Jayasekara, M. P.; Zhang, G.; Ackerson, C. J.; Kruhlak, M. J.; Leapman, R. D. Synthesis, Characterization, and Direct Intracellular Imaging of Ultrasmall and Uniform Glutathione-Coated Gold Nanoparticles. *Small* **2012**, *8*, 2277−2286.
(47) Chapman, R. E.; Munro, S. Retrieval of TGN Proteins from the Cell Surface Requires Endosomal Acidification. *EMBO J.* **1994**, *13*, 2305−2312.
(48) Puertollano, R.; Alonso, M. A. MAL, an Integral Element of the Apical Sorting Machinery, is an Itinerant Protein That Cycles Between the Trans-Golgi Network and the Plasma Membrane. *Mol. Biol. Cell* **1999**, *10*, 3435−3447.
(49) Meng, H.; Xue, M.; Xia, T.; Zhao, Y. L.; Tamanoi, F.; Stoddart, J. F.; Zink, J. I.; Nel, A. E. Autonomous in Vitro Anticancer Drug Release from Mesoporous Silica Nanoparticles by pH-Sensitive Nanovalves. *J. Am. Chem. Soc.* **2010**, *132*, 12690−12697.
(50) Mosure, K. W.; Henderson, A. J.; Klunk, L. J.; Knipe, J. O. Disposition of Conjugate-Bound and Free Doxorubicin in Tumor-Bearing Mice Following Administration of a BR96-Doxorubicin Immunoconjugate (BMS 182248). *Cancer Chemother. Pharmacol.* **1997**, *40*, 251−258.

DOI: 10.1021/acsami.5b04031
ACS Appl. Mater. Interfaces 2015, 7, 17171−17180